ChemPhysChem

Research Article
doi.org/10.1002/cphc.202300768

Chemistry Europe
European Chemical Societies Publishing

www.chemphyschem.org

Ab initio molecular dynamics of solvation effects and reactivity at the interface between water and ascorbic acid covered anatase TiO_2 (101)

Ida Ritacco,*[a] Gianluca Gatta,[b] Lucia Caporaso,[a] and Matteo Farnesi Camellone*[c]

In this work, we present a detailed study of the interaction between ascorbic acid (L-asc) and anatase TiO_2 (101) surface both in gas phase and in contact with water by using density functional theory and ab initio molecular dynamics simulations. In gas phase, L-asc strongly binds the TiO_2(101) surface as a dianion (L-asc^{2-}), adopting a bridging bidentate coordination mode (BB), with the two acid protons transferred to two surface 2-fold bridging oxygens (O2c). AIMD simulations show that the interaction between the organic ligand and the anatase surface is stable and comparable to the vacuum one despite the possible solvent effects and/or possible structural distortions of the ligand. In addition, during the AIMD simulations hydroxylation phenomena occur forming transient H_3O^+ ions at the solid-liquid interface. For the first time, our results provide insight into the role of the ascorbic acid on the electronic properties of the TiO_2 (101), the influence of the water environment on the ligand-surface interaction and the nature of the solid-liquid interface.

Introduction

Industrial products are the main responsible for environmental pollution by releasing their toxic waste into bodies of water, land, and air.[1–4]

Photocatalysis represents one of the most promising techniques for removal of environmental pollutants which, through oxidation-reduction processes, allow the degradation of the contaminants into less toxic reaction products, such as water and carbon dioxide.[5] In particular, heterogeneous photocatalysis is an effective and economical method for the degradation of air and water pollutants[6,7] by using a combined low-energy UV irradiation and semiconductor photocatalysts. Among different photocatalysts, TiO_2 has shown high performances in the photocatalytic degradation of air and water contaminants due to its peculiar properties, such as chemical stability, no toxicity and excellent adsorbent surface properties.[8–12] During the degradation processes, following a proper activation treatment as UV irradiation (photocatalysis), the electron–hole pairs trapped on metal/oxides surfaces react with adsorbed acceptors (oxygen) and donors (water) molecules forming highly reactive oxygen species (ROS), which are directly involved in the degradation of contaminants adsorbed on the surface.[7,13,14] In particular, the formation of the hydroxyl radical ($^{\bullet}OH$) seems to be favored on anatase TiO_2 whereas that of the superoxide anion radical ($O_2^{\bullet-}$) on rutile TiO_2.[14–16]

However, despite the high performance of TiO_2, the photocatalytic degradation of some organic pollutants is slow due to i) the TiO_2 bandgap (3.2 eV)[17,18] not accessible to the weak UV radiation, ii) the fast hole-electron recombination and iii) the low surface coverage of the photocatalyst.

Therefore, in recent years research has attempted to improve the photocatalytic performance of TiO_2 by using different techniques such as the doping of the metal/oxide with metallic[19,20] and non-metallic species,[17,18] the construction of heterojunctions with other oxides[21–25] and the adsorption of suitable organic chelating ligands, generating, in this last case, hybrid systems.[26–29] In fact, it is known that the use of organic ligands improves the pollutants adsorption on the surface,[17] slows down electronic recombination,[17] reduces the TiO_2 bandgap[26] and stabilizes the ROS formation[26] thus increasing the photocatalytic performance of the photocatalyst.

Experimental studies have shown that the photocatalytic activity of TiO_2 increases significantly when the coordinating organic ligand is the natural compound L-ascorbic acid (L-asc) due to the formation of a Ligand-to-Metal Charge Transfer (LMCT) complex.[30–33] Ascorbic acid, also known as Vitamin C, is a furan-based lactone of 2-ketogluconic acid containing an adjacent enediol adjacent to the carbonyl. Although it is experimentally known that the coordination of L-ascorbic acid improves the photocatalytic performance of TiO_2, a detailed understanding of the mechanisms leading to such improvements at atomistic level is needed.

[a] Dr. I. Ritacco, Prof. L. Caporaso
Dipartimento di Chimica e Biologia, Università degli Studi di Salerno, via Giovanni Paolo II 132, 84084 Fisciano, Salerno, Italy
E-mail: iritacco@unisa.it

[b] Prof. G. Gatta
Dipartimento di Medicina di Precisione Divisione di Radiologia, Università della Campania Luigi Vanvitelli, Napoli, Italia 80131

[c] Dr. M. Farnesi Camellone
CNR-IOM, Consiglio Nazionale delle Ricerche – Istituto Officina dei Materiali, c/o SISSA, 34136 Trieste, Italy
E-mail: farnesi@cnr.iom.it

Supporting information for this article is available on the WWW under https://doi.org/10.1002/cphc.202300768

Previous theoretical studies, in which the interaction of ascorbic acid with TiO_2 nanoparticles was investigated by cluster modeling, suggested that the ligand can adsorb on the nanoparticle in anionic form assuming parallel and/or perpendicular orientations and preferring the surface penta-coordinated titanium atoms as more stable binding sites.[34–36] Since this modeling type has many limitations, we decided to perform periodic DFT calculations in order to provide more accurate information on the gas phase interaction between ascorbic acid and anatase (101) surface. The first aim of our work was to clarify how L-asc improves the electronic properties of the photocatalyst. Our results demonstrate that the coordination of L-asc to $ATiO_2$ (101) generates a charge transfer from the ligand to the surface (LMCT) and a decrease of the bandgap.

Since water is regularly present in ambient reaction conditions, we also investigated the synergistic interaction of ascorbic acid, at low and high ligand coverage percentage, and water with the anatase (101) surface by ab initio molecular dynamics (AIMD) simulations. In fact, despite in literature experimental and theoretical studies relative to solid-liquid interfaces in presence of organic ligand such as carboxylic acids are available,[37–42] few information on the interaction of the ascorbic acid with $ATiO_2$ (101) surface in water environment are present.

With our simulations, performed for comparison purposes at different temperatures and at different L-asc coverage percentages, we clarify the effects of the water on the organic ligand-surface interaction and the nature of the solid-liquid interface interactions, demonstrating the stability of the ligand-surface bond despite the water presence in the reaction environment. Therefore, based on these results, we can affirm for the first time that the ascorbic acid-$ATiO_2$ (101) system could be an excellent candidate for various applications even when water is present in the reaction environment.

Computational Details

The spin-polarized DFT calculations were performed using CP2K[43] software package, which adopts a mixed Gaussian and plane-wave basis set (GPW).[43] The exchange-correlation potential was treated with the generalized gradient approximation parameterized by the Perdew-Burke-Ernzerhof functional.[44] For all atoms, a double ζ basis set[45] was employed in combination with the plane wave basis set with a density cut-off of 500 Ry and Goedecker-Teter-Hutter (GTH) pseudopotentials.[46] Brillouin zone integration was performed with a reciprocal space mesh consisting of only the Γ point and Van der Waals interactions were explicitly considered using the nonlocal rVV10 van der Waals functional.[47–49]

Periodic slab of $ATiO_2$ (101) was modeled by using a tetragonal (3×4) supercell with three TiO_2 layers for a total of 216 atoms. Between consecutive slabs a vacuum separation of 32 Å along *z* direction was entered.

In gas phase, the interaction of the L-ascorbic acid and the water with $ATiO_2$ (101) was investigated considering the organic ligand in all its possible protonated states, Molecular (L-asc, M), Mono-Anionic (L-asc$^-$, MA) and Di-Anionic (L-asc^{2-}, DA),[50] and the water in its molecular (M) and dissociated (D) form.[51] After the interaction with L-ascorbic acid and water, the system consists of 236 and 219 total atoms, respectively.

The adsorption energy of L-ascorbic acid and water was computed using the formula $E_{ads} = E_{SURF/L\text{-}asc(H2O)} - (E_{SURF} + E_{L\text{-}asc(H2O)})$, where $E_{SURF/L\text{-}asc(H2O)}$ is the energy of the combined system (namely the surface plus L-ascorbic acid(water)), E_{SURF} is the energy of the stoichiometric surface alone ($E_{ATiO2(101)}$), and $E_{L\text{-}asc(H2O)}$ is the energy of the L-ascorbic acid(water) in gas phase.

The charge analysis was performed following the Bader's theory since the charge enclosed within the Bader volume can be considered a good approximation of the total electronic charge of an atom.[52–54] The differences between the Bader charges of the coordinated and free L-ascorbic acid (Δq, e^-) were calculated according to the equation $\Delta q = \Sigma q(SURF/L\text{-}asc) - \Sigma q(L\text{-}asc)$, where $\Sigma q(SURF/L\text{-}asc)$ is the sum of the Bader charges of L-ascorbic acid adsorbed on stoichiometric anatase surface, while $\Sigma q(L\text{-}asc)$ is the sum of the Bader charges of the free L-ascorbic acid.

We employed ab initio molecular dynamics (AIMD) to investigate the solvent-induced structural effects occurring at the interface between the L-ascorbic acid adsorbed on the $ATiO_2$ (101) surface (L-asc/$ATiO_2$) and liquid water. The Born-Oppenheimer AIMD simulations were also performed with CP2K[43] software package by using the computational protocol adopted for the gas phase calculations. To create the interface between the L-asc/$ATiO_2$ and water, the space between the slabs was fully filled with 80 H_2O molecules which, considering the size of the systems, allow a better description of the solvent phase in reasonable calculation times. Purely for comparison purposes, the canonical NVT ensemble was employed with a target temperature of 350 K and 450 K, which seem to better simulate the structural properties of water at room temperature,[55–57] using the "canonical sampling velocity rescaling" thermostat proposed by Bussi and co-workers.[58] An integration time step of 0.5 fs was adopted and the mass of the hydrogen atoms was replaced by deuterium to allow for a larger time step. The AIMD simulations were run for a production phase of 20 ps, a more than enough duration for AIMD of complex systems like ours which allows for meaningful and satisfying statistics.[55,59–61]

Results and Discussion

Interaction of ascorbic acid and $ATiO_2$ (101) in gas phase

First, we performed a set of DFT calculations in vacuum to investigate the most stable adsorption structures of L-ascorbic acid on the stoichiometric anatase TiO_2 (101) surface. Different protonation states of the L-ascorbic acid were considered: Molecular (L-asc, M), Mono-Anionic (L-asc$^-$, MA) and Di-Anionic (L-asc^{2-}, DA) (see Figure 1a, b and c, respectively).[50] The anatase TiO_2 (101) surface (Figure S1 of the Supporting Information (SI)) exposes both fully undercoordinated 5-fold Ti^{4+} (Ti5c) and 2-fold bridging oxygens (O2c).[26,62,63] Molecular ligand can interact with the surface in Parallel (M-P) or in Bridging Bidentate (M-BB) conformations (Figure 1d and e). Whereas the anionic species bind to the undercoordinated Ti5c atoms in Mono-Anionic Monodentate (MA-M) and Di-Anionic Bridging Bidentate (DA-BB) forms (Figure 1f and g). In the deprotonated structures MA and DA, the acid protons are transferred from L-asc to O2c atoms close to the ligand coordination sites, forming OH groups (O2c–Hs).

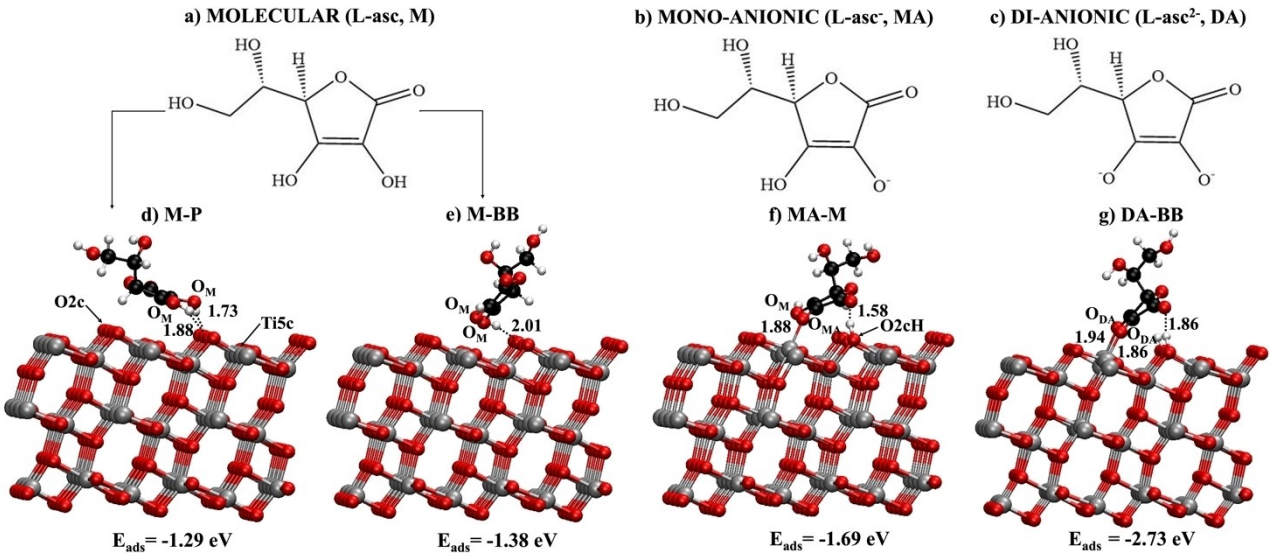

Figure 1. Protonation states of the L-ascorbic acid a) Molecular (M), b) Mono-anionic (MA) and c) Di-anionic (DA) and optimized structures of the interaction of L-ascorbic acid and $ATiO_2$ (101) with the ligand in d) Molecular Parallel (M-P), e) Molecular Bridging Bidentate (M-BB), f) Mono-Anionic Monodentate (MA-M) and g) Di-Anionic Bridging Bidentate (DA-BB) forms. The corresponding E_{ads} are reported in eV. Ti, C, H, and O surface and ligand atoms are represented in ball and sticks and depicted in gray, black, white, and red, respectively. Bond distances are reported in Angstrom (Å).

The optimized geometries together with the corresponding adsorption energies (E_{ads}) are reported in Figure 1.

In M-P and M-BB structures (Figure 1d and e), L-asc interacts with $ATiO_2$ (101) establishing H-bonds between the hydroxyl groups adjacent to the alkene moiety of the ligand and the O2c atoms of the surface. In M-P conformation, where the furan moiety of ascorbic acid interacts with the stoichiometric anatase (101) surface, there are two H-bonds of 1.73 and 1.88 Å, respectively (Figure 1d), while in M-BB only one of 2.01 Å is formed (Figure 1e). The M-BB E_{ads} is −1.38 eV and it turns out to be slightly better than that reported for M-P (−1.29 eV) of about 0.1 eV most likely due to the interaction of the ligand oxygen atoms O_M with two 5-fold Ti^{4+} of the surface.This interaction does not occur in M-P in which the ligand interacts with the surface in a planar manner (compare E_{ads} for M-P and M-BB configurations reported in Figure 1d and e, respectively).

In MA-M configuration (Figure 1f), the deprotonated oxygen atom (O_{MA}) of the mono-anionic ligand (L-asc$^-$) coordinates to the penta-coordinated Ti5c atom of the surface in the monodentate mode, forming a new Ti5c–O_{MA} bond of 1.88 Å. The adsorption energy (E_{ads}), associated with this structure and enhanced by the formation of a H-bond between the carbonyl oxygen of the ligand and one of the two O2c–H groups of the surface of 1.58 Å, turns out to be −1.69 eV. The most stable structure is the DA-BB one with E_{ads} of −2.73 eV. In this configuration the L-ascorbic acid coordinates to the $ATiO_2$ (101) surface in its doubly deprotonated form (L-asc^{2-}) adopting a bridging bidentate coordination mode (BB) with the two deprotonated oxygen atoms (O_{DA}) bonded to two penta-coordinated Ti5c atoms of the surface. The computed lengths of the two newly formed Ti5c–O_{DA} bonds are found to be 1.86 and 1.94 Å (Figure 1g). Similarly to MA-M conformation, also in this case the adsorption of the ascorbate on the surface is strengthened by the formation of the H-bond between the carbonyl oxygen of the ligand and one of the two O2c–H groups of the surface, 1.86 Å long (Figure 1g).

Bader charge analysis, computed on the most stable DA-BB configuration as the difference between the Bader charges (Δq, e^-) of the L-asc atoms in $ATiO_2$-bound and free forms, reveals that the interaction between L-asc^{2-} and the anatase (101) surface induces a charge transfer from the organic ligand to $ATiO_2$ of $0.7|e^-|$, indicative of a Ligand-to-Metal Charge Transfer (LMCT) (see Table S1 of the SI). In addition, the PDOS plots of the $ATiO_2$ (101) and the DA-BB model, reported in Figure S2 of the SI, show a bandgap of 2.4 and 2.0 eV, respectively, Therefore, our results suggest that the presence of Di-Anionic ascorbate contributes to reduce the $ATiO_2$ surface bandgap.

Generally, in the degradation processes water is regularly present. For this reason, the adsorption energy of the water molecule, in its molecular and dissociated form,[51] was computed (E_{ads} in Figure 2a and b, respectively) and compared with the E_{ads} obtained for the L-ascorbic acid in its molecular and mono-anionic form (E_{ads} in Figure 1e and f, respectively) to understand if the water adsorption can compete with the ligand one.

In molecular adsorption, water interacts with the anatase (101) surface by forming a dative bond between the water oxygen (O_w) and a Ti5c site of 2.25 Å and two H-bonds between the water hydrogens (H_{w1} and H_{w2}) and two O2c sites of 2.22 and 2.11 Å, respectively, with an E_{ads} of −1.12 eV (Figure 2a). In the dissociative adsorption, the O_wH_{w2} group binds covalently a Ti5c site at 1.84 Å, while H_{w1} coordinates an O2c site at 0.99 Å with an E_{ads} of −0.67 eV (Figure 2b).

Our results indicate that the molecular adsorption is more stable than the dissociative one by 0.45 eV, in line with the reference 51. In the dissociative adsorption the formation of the covalent bond between the O_wH_{w2} group and the Ti5c site causes an elongation of the O3c-Ti5c bond by 0.33 Å, passing

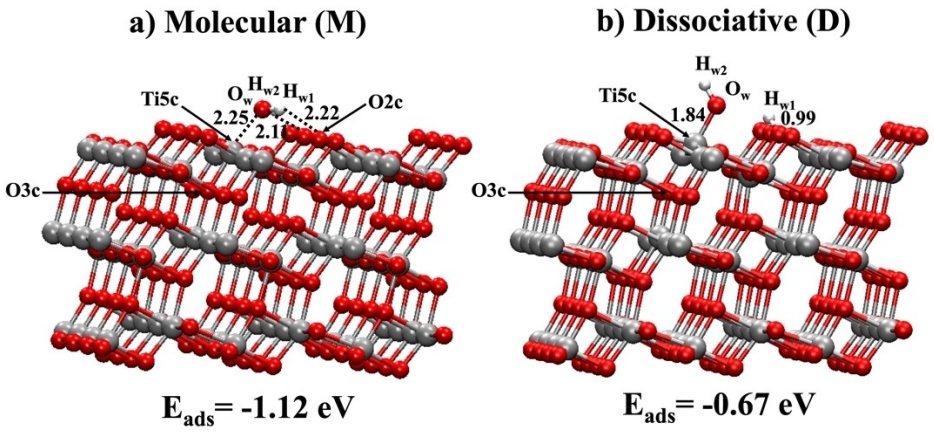

Figure 2. a) Molecular (M) and b) Dissociative (D) adsorption of the water molecule. The corresponding E_{ads} are reported in eV. Ti, O and H atoms are represented in ball and sticks and depicted in gray, red and white, respectively. Bond distances are reported in Angstrom (Å).

from 1.87 Å in the molecular adsorption to 2.20 Å when the water is in its dissociated form (Figure 2a and b), destabilizing the dissociative adsorption.

In addition, comparing the E_{ads} of the molecular and dissociative water adsorption (E_{ads} in Figure 2a and b, respectively) with the E_{ads} of the L-ascorbic acid adsorption in its molecular and Mono-Anionic form (E_{ads} in Figure 1e and f, respectively), we can confirm that the organic ligand adsorbs more strongly than water by about 0.3 and 1.0 eV for the molecular and anionic form, respectively. Therefore, the water adsorption does not compete with the adsorption of the L-ascorbic acid.

Since no studies on the stability of the interaction between L-ascorbic acid and $ATiO_2$ (101) surface in water environment are available, we performed AIMD simulations to the most stable DA-BB configuration (Figure 1g), considering the adsorption of one and two Di-anionic ascorbates in order to explore the "ligand coverage percentage" and the solvent effects on the interaction of L-asc and water with the anatase. Considering that the surface Ti atoms are 24, the ligand coverage percentages are approximately 4% and 8%, respectively.

Interaction of one ascorbic acid with $ATiO_2$ (101) in water environment

We performed AIMD simulations at T = 350 and 450 K aimed to investigate solvent effects on ascorbic acid molecules adsorbed on $ATiO_2$ (101) surfaces in contact with liquid water.

Let us start by considering the DA-BB adsorption mode of one ascorbic acid on anatase (101) under wet conditions. In DA-BB mode, the ascorbic acid is Di-Anionic and two O2c–H groups are present on the $ATiO_2$ (101) surface (yellow and green atoms in Figure 3 and 4). Since the O2c–H groups may occupy different positions on the metal/oxide surface, we considered two starting configurations for the AIMD simulations: a first one with the two O2c–H groups close to the adsorbed ascorbate molecule ($\mathbf{I_C}$) and a second one where the O2c–H groups are far from the ligand ($\mathbf{I_F}$) (Figure S3a and S3b of the SI).

To evaluate the interaction between L-asc^{2-} and the $ATiO_2$ support at the water interface, we monitored the time evolution of the Ti5c–O_{DA} and O2c–H bond lengths along the AIMD trajectories (20 ps) for both $\mathbf{I_C}$ (Figure 3) and $\mathbf{I_F}$ (Figure 4) systems at 350 and 450 K.

The representative snapshots of the equilibrated interface structure of $\mathbf{I_C}$ system resulting from the AIMD simulations at 350 and 450 K are reported in Figure 3a and c, respectively. The average lengths computed for Ti5c–O_{DA} and O2c–H bonds of $\mathbf{I_C}$ system at 350 and 450 K (Figure 3b and d, respectively), reported in Table 1, suggest that, within the time scale of our simulations, the L-asc^{2-} adsorption is stable even in water presence. However at 350 K, in the solvated system, one of the two Ti5c–O_{DA} bonds undergoes a considerable elongation with respect to the bond lengths in gas-phase (see caption of Table 1 and Figure 1g) due to the structural distortion of the ascorbate which is accentuated in solvent to preserve the H-bond between the carbonyl oxygen of the ligand and one of the two surface hydrogens O2c–H (yellow atom in Figure 3a), already present in vacuum (compare Figure 3a and Figure 1g). At higher temperatures, this hydrogen bond is not conserved (compare Figure 3a and c and Figure S4 of the SI). Therefore, during the AIMD simulations at 450 K, the ascorbate loses its initial structural distortion interacting with the anatase surface via shorter Ti5c–O_{DA} bond distances (see Table 1 and Figure 3c).

The O2c–H bonds are the same at 350 K and 450 K (Table 1), suggesting that they are not affected by the water environment.

Table 1. The average lengths computed for Ti5c–O_{DA} and O2c–H bonds of $\mathbf{I_C}$ system at 350 and 450 K reported in Angstrom (Å).

Ic system bonds distance (Å)	*Ti5c–O_{DA}	O2c–H
350 K	1.93 ± 0.06 2.26 ± 0.23	0.99 ± 0.03 0.99 ± 0.03
450 K	1.96 ± 0.08 2.05 ± 0.09	0.99 ± 0.03 0.99 ± 0.03

* The Ti5c–O_{DA} bonds in gas phase are 1.86 and 1.94 Å, respectively.

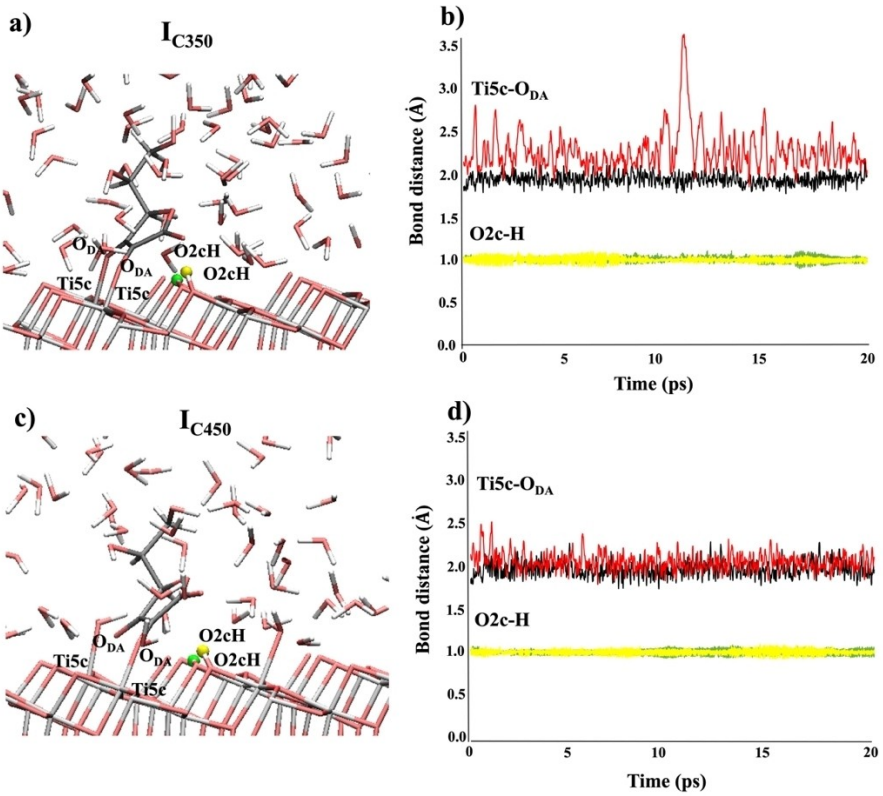

Figure 3. Representative snapshots of the equilibrated interface structure of $\mathbf{I_C}$ system resulting from the AIMD simulations at a) 350 K and c) 450 K, respectively. In a) and c) Ti, C, H, and O are represented in licorice and depicted in gray, black, white, and red, respectively. Whereas the H atoms of the O2c–H groups are in ball and sticks and depicted in green and yellow. Time evolution plots of the Ti5c–O_{DA} and O2c–H bond lengths for $\mathbf{I_C}$ along the AIMD trajectories (20 ps) at b) 350 K and d) 450 K, respectively. In b) and d) the red and black lines indicate the Ti5c–O_{DA} bonds while the yellow and green lines indicate the O2c–H bonds.

In $\mathbf{I_F}$ system, the O2c–H groups, resulting from the adsorption and deprotonation of L-asc on the metal/oxide surface, are locate far from the molecule (Figure 4).

At 350 K, the interaction of $ATiO_2$ with the aqueous interface leads to the partial surface hydroxylation by means of the barrierless dissociation of an interfacial water molecule (H_2O_{w1}). The analysis of the AIMD trajectory, of which a representative snapshot is reported in Figure 4a together with a plot of the time evolution of the bond lengths of all atoms involved in the process (Figure 4b), shows that the dissociation of the interfacial water molecule H_2O_{w1} occurs after about 7 ps by the transfer of the H_{w1} proton (purple atom in Figure 4a) to the closest water molecule H_2O_{w2} (blue atom in Figure 4a). Simultaneously, the H_{w2} proton (pink atom in Figure 4a) moves from H_2O_{w2} to the closest surface O2c atom (blue atom in Figure 4a), leading to the formation of an additional surface OH group (O2c–H) and of the solvated hydroxide HO_{w1} (purple and pink lines in Figure 4b), in agreement with previous theoretical studies on oxide surfaces.[59,64–69]

At 450 K, the time evolution plot of the O2c–H bond lengths (Figure 4e) shows that both surface O2c–H groups bond distances increase significantly after 18 and 19 ps of simulation time (green and yellow lines in Figure 4e), suggesting that the two protons adsorbed on the O2c surface diffuse into the aqueous interface to form transient H_3O^+ ions near the interface, according to other previous theoretical studies.[42,70,71] In particular, during the simulation the two O2c–H protons, indicated in green and yellow in Figure 4d, interacts with interfacial water molecules H_2O_{w1} and H_2O_{w2} (blue atoms in Figure 4d) respectively, forming the two H_3O^+ ions. Simultaneously, the two protons from H_3O^+ ions, indicate in cyan and orange in Figure 4d, move to the closest surface O2c atoms (blue atom in Figure 4d), forming two new additional surface O–H groups (O2c–H) and restoring the starting situation (green, yellow, cyan and orange lines in Figure 4e).

Therefore, when the O2c–H groups are far from the L-asc^{2-} at 450 K the formation of H_3O^+ ions, albeit transitory, is observed. Most likely in the $\mathbf{I_C}$ systems, where the O2c–Hs are very close to the ligand coordination sites, the H_3O^+ formation is prevented by the large dimensions of the ligand and by the structural distortions that L-asc^{2-} undergoes during the simulations to establish H-bonds with neighboring O2c–Hs.

The average lengths computed for the $\mathbf{I_F}$ Ti5c–O_{DA} bonds of at 350 and 450 K (Figure 4c and f, respectively), reported in Table 2, indicate that at both temperatures the L-asc^{2-} adsorption is more stable than the $\mathbf{I_C}$ systems, with Ti5c–O_{DA} bond distances almost comparable to those computed in the gas-phase case (see caption of Table 2 or Figure 1g). In the $\mathbf{I_F}$ system, where O2c–Hs are far from the molecule, the stronger ligand-surface interaction can be traced back to the absence of

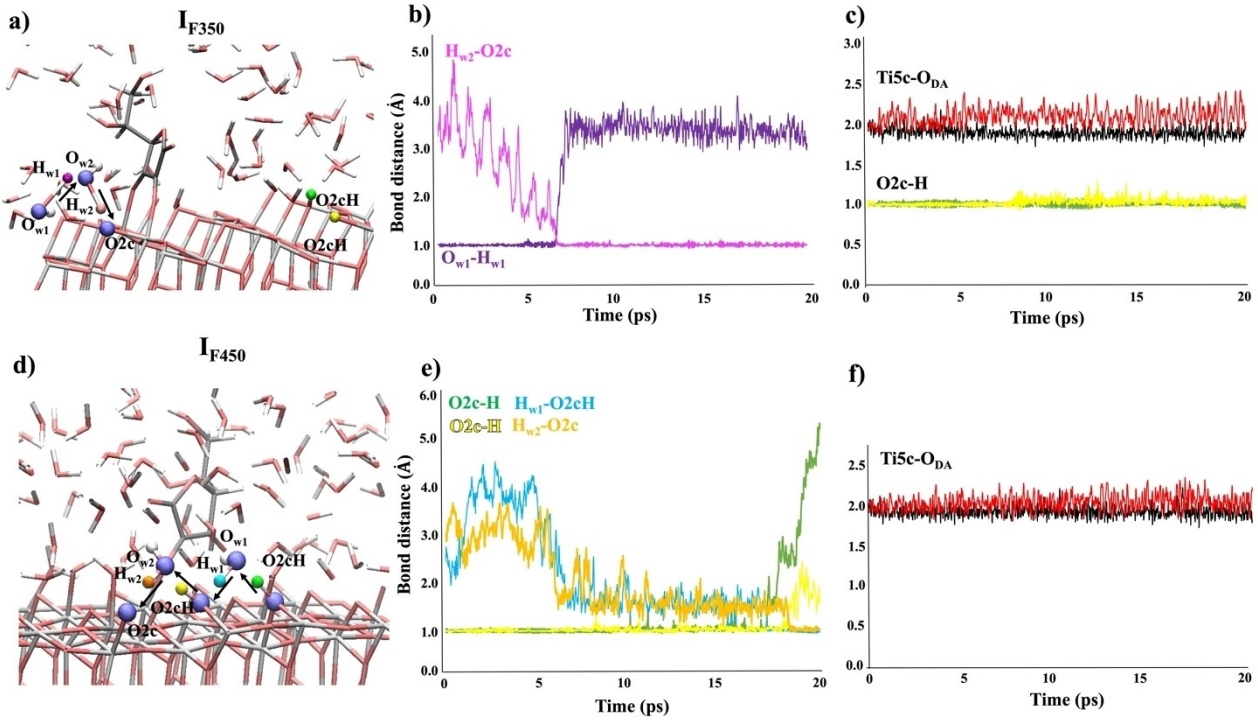

Figure 4. a) and d) Representative snapshots of the equilibrated interface structure of $\mathbf{I_F}$ system resulting from the AIMD simulations at 350 and 450 K, respectively. Time evolution plots of the O2c–H and Ti5c–O_{DA} bond lengths for $\mathbf{I_F}$ along the AIMD trajectories (20 ps) at b) and c) 350 K and e) and f) 450 K, respectively. In a) and d) Ti, C, H, and O are represented in licorice and depicted in gray, black, white, and red, respectively. In both snapshots, the H atoms of the O2c–H groups are in ball and sticks and depicted in green and yellow. In a) the oxygen atoms of the water molecules involved in the hydroxylation phenomena (O_{w1} and O_{w2}), the surface O2c and the H atoms involved in the proton transfer (H_{w1} and H_{w2}) are represented in ball and sticks and depicted in blue, purple and pink, respectively. In d) the oxygen atoms of the water molecules involved in the H_3O^+ formation (O_{w1} and O_{w2}), the surface O2c, the H atoms involved in the proton transfer (H_{w1} and H_{w2}) and the H atoms of the O2c–H groups are represented in ball and sticks and depicted in blue, cyan, orange, green and yellow. In b) the purple and pink lines indicate the O_{w1}–H_{w1} and H_{w2}–O2c bonds, respectively. In c) and f) the red and black lines indicate the Ti5c–O_{DA} bonds. In c) the yellow and green lines indicate the O2c–H bonds. In e) the yellow and green lines indicate the O2c–H bonds, while the cyan and orange lines indicate H_{w1}–O2cH and H_{w2}–O2c bonds.

Table 2. The average lengths computed for Ti5c–O_{DA} bonds of $\mathbf{I_F}$ system at 350 and 450 K reported in Angstrom (Å).

$\mathbf{I_F}$ system bonds distance (Å)	*Ti5c–O_{DA}
350 K	1.87 ± 0.06 2.09 ± 0.10
450 K	1.91 ± 0.06 2.02 ± 0.09

* The Ti5c–O_{DA} bonds in gas phase are 1.86 and 1.94 Å, respectively.

ascorbate structural distortions, which instead occur in the $\mathbf{I_C}$ systems due to the presence of H-bond between carbonyl oxygen atom of the ligand and surface OH groups and to the lower solvent effects.

In addition, the different behavior of the $\mathbf{I_F}$ systems at 350 and 450 K can be explained in detail by the average Ti5c–O_{DA} bond lengths (see Figure 5). In fact, at 350 K the formation of a strong Ti5c–O_{DA} bond (1.87 ± 0.06 Å) weakens the surface Ti5c–O2c and O2c-Ti5c bonds close to the ligand coordination site (1.98 ± 0.11 Å and 2.01 ± 0.11 Å, respectively) (Figure 5a and Figure S5 of the SI). This favors the interaction of the O2c atom with the interfacial water molecule, the dissociation of the latter and the protonation of the anatase surface.

At 450 K, where the Ti5c–O_{DA} bonds are slightly longer (1.91 ± 0.06 Å), the surface Ti5c–O2c and O2c-Ti5c bonds are stronger (1.88 ± 0.07 Å and 1.89 ± 0.08 Å, respectively) preventing the protonation of the surface external layer (Figure 5b and Figure S5 of the SI).

Figure 6 shows a plot of the planar average profile of the water density as a function of the distance from the $ATiO_2$ (101) surface for $\mathbf{I_C}$ systems at 350 and 450 K, respectively.

As shown in Figure 6a' and 6b', the average water density profiles show a first peak at ~3.0 Å above the $ATiO_2$ (101) surface corresponding to H_2O molecules interacting with the surface Ti5c sites. This peak is slightly more pronounced in the AIMD simulation at 450 K (Figure 6b') suggesting an increase of the solvent density at the interface. The subsequent broader peaks are indicative of the H-bonds that the H_2O molecules form with the surface O2c atoms.

In $\mathbf{I_F}$ systems at 350 and 450 K the different position of the O–H groups on the surface does not change the water structure. Snapshots and the average water density profiles for $\mathbf{I_F}$ at 350 K and 450 K are reported in Figure S6 of the SI.

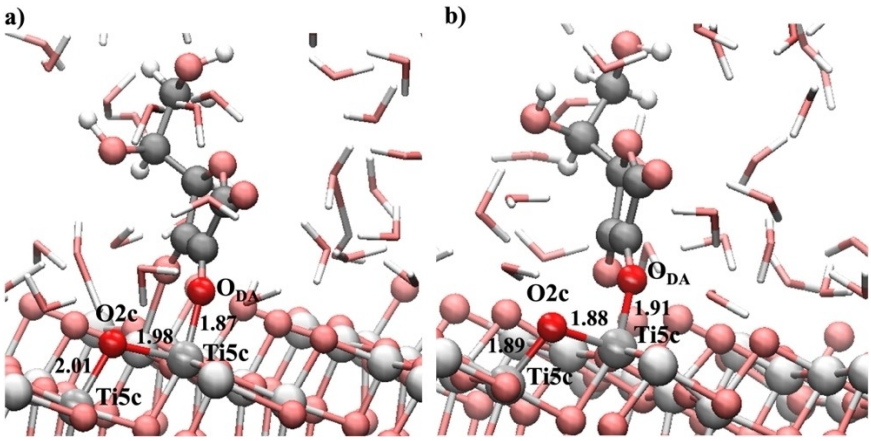

Figure 5. Ti5c–O_{DA} and Ti5c–O2c bond distances in $\mathbf{I_F}$ at a) 350 and b) 450 K. Ti, C, H, and O surface and ligand atoms are represented in ball and sticks and depicted in gray, black, white, and red, respectively. H and O water atoms are represented in licorice and depicted in white and red. Bond distances are reported in Angstrom (Å).

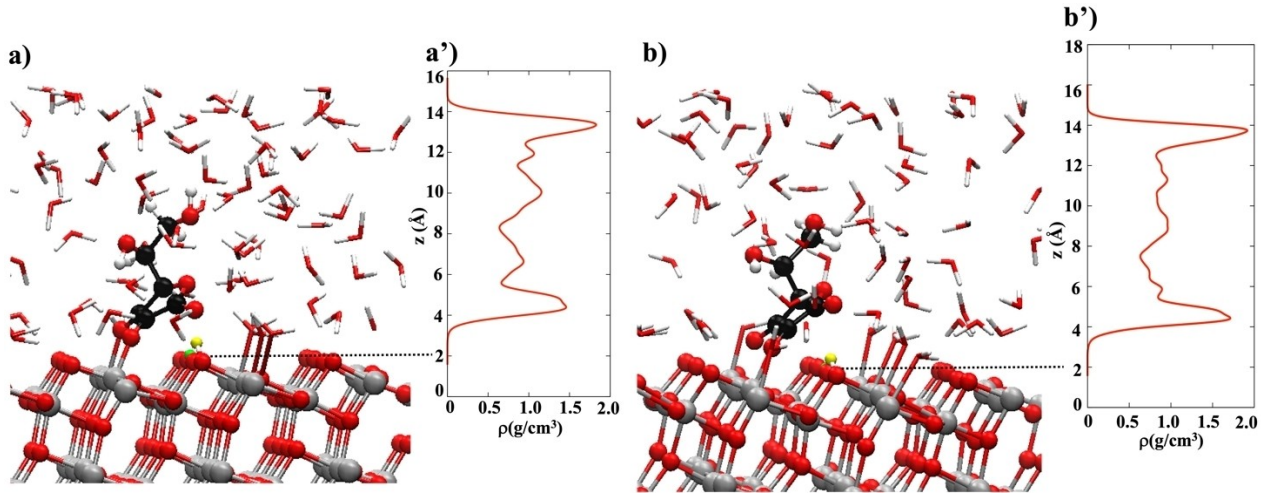

Figure 6. a), b) Snapshots and a'), b') water density profiles for $\mathbf{I_C}$ system resulting from the AIMD simulations at 350 and 450 K. In a) and b) Ti, C, H, O and H atoms of the O2c–H groups are represented in ball and sticks and depicted in gray, black, white, red, green and yellow, respectively. H and O water atoms are represented in licorice and depicted in white and red.

Interaction of two ascorbic acid with $ATiO_2$ (101) in water environment

Next, we focused on the adsorption of two ascorbic acid on anatase (101) under wet conditions. Two structures were considered as starting point for AIMD simulations at 350 K (see Figure 7a and 7b). In both structures, the two ascorbic acid molecules are present on the $ATiO_2$ (101) surface in the preferred DA-BB adsorption mode, discussed before, but in a) the two molecules are close to each other (**2DA-BB_close**), whereas in b) the molecules are faraway (**2DA-BB_far**).

The AIMD simulations were also carried out at 450 K. In the latter, the results were no different from those obtained at 350 K and, therefore, they will not be reported in this work.

In **2DA-BB_close** (Figure 8a), the breaking of one of the four O–H bonds present on the surface (ochre atom in Figure 8a) occurs after about 2 ps of simulation time. The proton deriving from this breakage moves on the neighboring interfacial water molecule H_2O_{w1} (blue atom in Figure 8a), forming a H_3O^+ ion (ochre and light blue lines in Figure 8b). At this point, the H_3O^+ ion, that is formed at the solid-liquid interface, diffuses into the aqueous bulk through consecutive transient proton transfers. In fact, from H_3O^+, H_{w1} (pink atom in Figure 8a) moves on neighboring water molecule H_2O_{w2} (blue atom in Figure 8a) and subsequently H_{w2} (orange atom in Figure 8a) on H_2O_{w3} (blue atom in Figure 8a). In **2DA-BB_far** (Figure 8d), the formation of the transient H_3O^+ ion occurs after 5 ps of simulation time by the transfer of one of the four protons adsorbed on the surface (yellow atom in Figure 8d) on the neighboring interfacial water molecule H_2O_{w1} (blue atom in Figure 8d). Simultaneously, the H_{w1} proton (cyan atom in Figure 8d) moves from H_3O^+ ion to the closest surface O2c atom (blue atom in Figure 8d), forming a new additional surface O–H group (O2c–H) and restoring the fourth superficial O2c–H group. Therefore, at 350 K, in both **2DA-BB_close** and **2DA-BB_far** system, the formation of transient H_3O^+ ions is observed, as suggested by the time

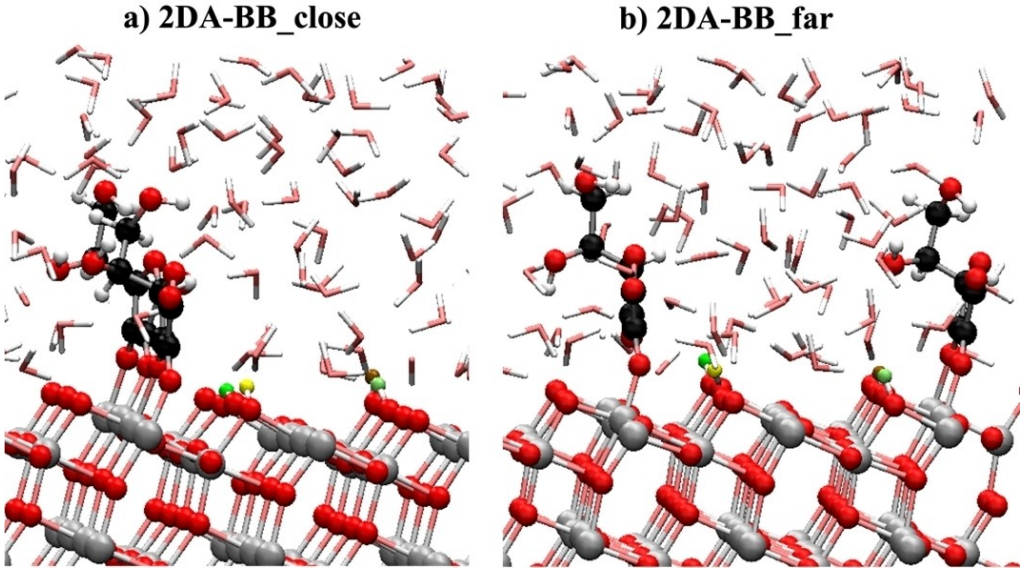

Figure 7. Interaction of two L-asc^{2-} a) close and b) far to each other in Bridging Bidentate (BB) configuration on $ATiO_2$ (101) in contact with water in presence of four O2c–H groups. Ti, C, H, and O surface and ligand atoms are represented in ball and sticks and depicted in gray, black, white, and red, respectively. H and O water atoms are represented in licorice and depicted in white and red, while the protons deriving from the acid ascorbic dissociation (O2c–H) are represented in ball and sticks and depicted in green, yellow, ochre and lime, respectively.

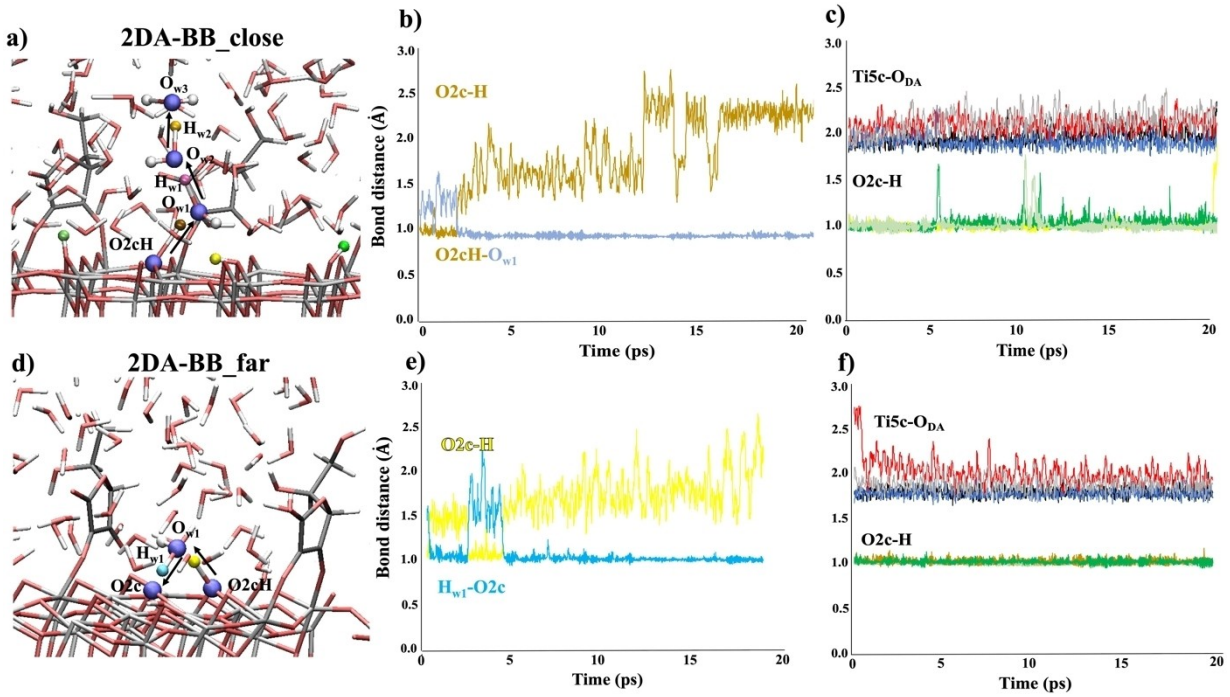

Figure 8. a) and d) Representative snapshots of the equilibrated interface structure of **2DA-BB_close** and **2DA-BB_far** systems resulting from the AIMD simulations at 350 K respectively. In **2DA-BB_close** the O2c–H proton involves in the H_3O^+ formation is represented in ochre (panel a), whereas in **2DA-BB_far** the O2c–H proton involves in the H_3O^+ formation is represented in yellow (panel d). In a) and d) Ti, C, H, and O are represented in licorice and depicted in gray, black, white, and red, respectively. In both snapshots, the H atoms of the O2c–H groups are in ball and sticks and depicted in green, yellow, ochre and lime, respectively. In a) the oxygen atoms of the water molecules involved in the H_3O^+ formation (O_{w1}, O_{w2} and O_{w3}), the surface O2c and the H atoms involved in the proton transfer (O2cH, H_{w1} and H_{w2}) are represented in ball and sticks and depicted in blue, ochre, pink and orange, respectively. In d) the oxygen atoms of the water molecule involved in the H_3O^+ formation (O_{w1}), the surface O2c, the H atom involved in the proton transfer (H_{w1}) and the H atoms of the O2c–H groups are represented in ball and sticks and depicted in cyan and yellow.

evolution plot of the O2c–H bond lengths reported in Figure 8b and e respectively.

Time evolution plots of the O2c–H and Ti5c–O_{DA} bond lengths for both systems along the AIMD trajectories (20 ps) at 350 K are reported in panels b), c) and e), f), respectively. In b)

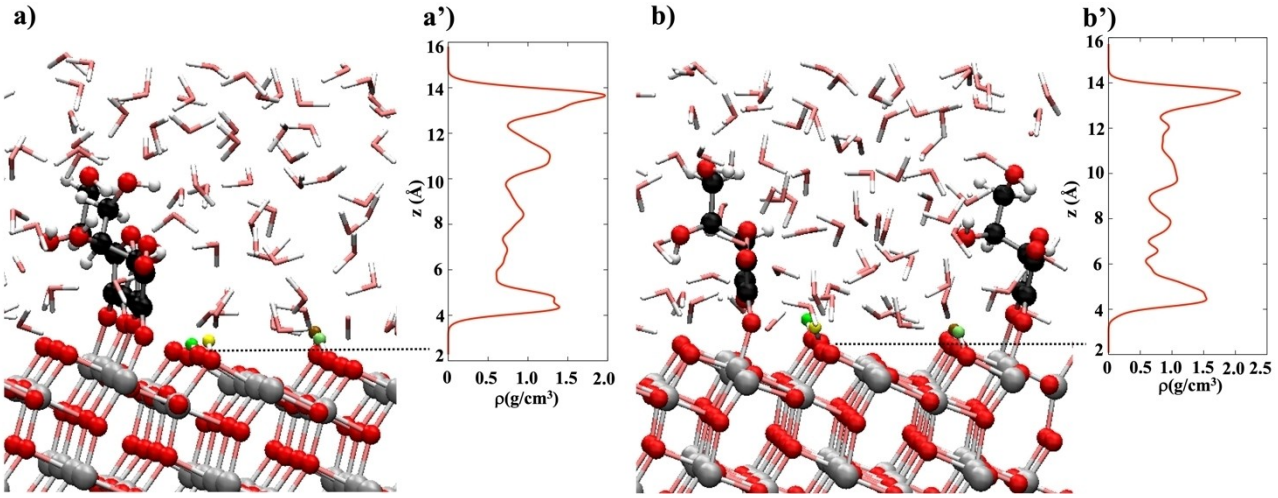

Figure 9. a), b) Snapshots and a'), b') water density profiles for **2DA-BB_close** and **2DA-BB_far** systems resulting from the AIMD simulations at 350 K. Ti, C, H, and O surface and ligand atoms are represented in ball and sticks and depicted in gray, black, white, and red, respectively. H and O water atoms are represented in licorice and depicted in white and red, while the protons deriving from the acid ascorbic dissociation (O2c–H) are represented in ball and sticks and depicted in green, yellow, ochre and lime, respectively.

the ochre and light blue lines indicate the breaking of the O2c–H and the formation of the O2cH–O_{w1} bonds, respectively. In e) the yellow and cyan lines indicate the breaking of the O2c–H and the formation of the H_{w1}–O2c bonds, respectively. In c) and f) the red, black, dark blue and gray lines indicate the Ti5c–O_{DA} bonds. In c) the yellow, green and lime lines indicate the O2c–H bonds, while in f) the ochre and green lines indicate the O2c–H bonds.

For both systems, the time evolution of the Ti5c–O_{DA} bond lengths (Figure 8c and f) was also monitored along the AIMD trajectories (20 ps) to evaluate the coverage effects on the L-asc^{2-} adsorption. The results, reported in Table 3, indicate that at higher coverage percentages Ti5c–O_{DA} distances are slightly shorter than those reported at lower percentages (see Table 1 and 2) and comparable to those obtained in gas-phase (see caption of Table 3 and Figure 1g). Also in this case, the effects of the solvent are low and the interactions between the ligand and the surface OH groups are absent as they are involved in the formation of H_3O^+ ions.

Table 3. The average lengths computed for Ti5c–O_{DA} bonds of **2DA-BB_close** and **2DA-BB_far** systems at 350 K reported in Angstrom (Å).

2DA-BB_close system bonds distance (Å)	*Ti5c–O_{DA}
350 K	1.96 ± 0.08 2.08 ± 0.09 1.91 ± 0.07 2.12 ± 0.12
2DA-BB_far system bonds distance (Å)	*Ti5c–O_{DA}
350 K	1.91 ± 0.06 2.18 ± 0.17 1.91 ± 0.06 2.02 ± 0.09

* The Ti5c–O_{DA} bonds in gas phase are 1.86 and 1.94 Å, respectively.

In fact, unlike low coverage percentage (4%), at high L-asc^{2-} coverage percentage (8%) the formation of the H_3O^+ ions is always observed. Most likely this occurs because at high coverage percentage the large dimensions of the ascorbic acid force the ligand into an almost perfectly perpendicular position to the surface, reducing the formation of those structural distortions which instead occur at low coverage percentage and which could, as already explained in the previous paragraph, block the formation of H_3O^+ ions.

Therefore, our simulations show that the formation process of the transient H_3O^+ ions, involving the transfer of the O2c–H protons adsorbed on the surface on neighboring interfacial water molecules, could be affected by the ascorbate coverage percentages and by the position of the O2c–H groups with respect to the ligand.

In Figure 9 are reported snapshots and the average water density profiles for **2DA-BB_close** and **2DA-BB_far**, respectively.

In both systems, the first broad and asymmetrical peak at ~3.0 Å is related to the partial hydration of the anatase external layer at the interface, while the subsequent broader peaks are indicative of the H-bonds that the H_2O molecules form with each other (Figure 9a' and 9b').

Conclusions

In this work, we provided a detailed analysis on the stability of the interaction between ascorbic acid and anatase TiO_2 (101) surface both in vacuum and in water environment.

In vacuum, the ascorbic acid presence causes a decrease of the bandgap and generates Ligand-to-Metal Charge Transfer (LMCT) phenomena.

Our AIMD simulations (20 ps) demonstrated that the water environment does not affect the ligand-surface interactions. In fact, both at low and high L-asc^{2-} coverage percentage (4%

and 8%, respectively) and regardless of the simulations temperature, the interaction between ascorbic acid and $ATiO_2$ (101) is stable in the time and even comparable with that obtained in vacuum, despite the possible solvent effects and the possible structural distortions of the ligand. The hydration and the hydroxylation of the external layer of the surface could be affected by the ascorbate coverage percentages and by the position of the O2c–H groups with respect to the ligand. In addition, in presence of two L-asc^{2-} is always observed the formation of H_3O^+ ions at the aqueous interface.

Therefore, the information obtained from our study highlights how the ascorbic acid/$ATiO_2$ (101) system can be used in specific applications and in different fields due to its efficiency in vacuum and its high stability in water environment.

Supporting Information

Description of the anatase TiO_2 (101) surface structure; Sum of the Bader charges of the ascorbic acid atoms in free and $ATiO_2$ bound form; PDOS and spin density plots for L-asc^{2-} on $ATiO_2$ (101) surface; Interaction of L-asc^{2-} in Bridging Bidentate configuration on $ATiO_2$ (101) in contact with water in presence of two O2c–H groups close and far from the organic ligand; Water density profiles for $\mathbf{I_F}$ system at 350 and 450 K.

Author Contributions

The manuscript was written through contributions of all authors. All authors have given approval to the final version of the manuscript.

Acknowledgements

For computer time, this research used the resources of the KAUST Super-computing Laboratory (KSL) at KAUST.

Conflict of Interests

The authors declare no conflict of interest.

Data Availability Statement

The data that support the findings of this study are available in the supplementary material of this article.

Keywords: TiO_2 surface · organic ligand · hybrid systems · DFT · AIMD · Photocatalysis

[1] G. Saxena, R. N. Bharagava, in *Environmental Pollutants and their Bioremediation Approaches* **2017**, CRC Press, 34.
[2] L. Liang, Z. Wang, J. Li, *J. Cleaner Prod.* **2019**, *237*, 117649.
[3] F. Dong, Y. Wang, L. Zheng, J. Li, S. Xie, *J. Cleaner Prod.* **2020**, *246*, 118960.
[4] H. Deng, R. Wei, W. Luo, L. Hu, B. Li, Y. Di, H. Shi, *Environ. Pollut.* **2020**, *258*, 113658.
[5] P. Pichat, G. Ertl, H. Knözinger, J. Weitkamp, in *Handbook of Heterogeneous Photo-Catalysis* **1997**, vol. 4, VCH, Weinheim, 2111.
[6] H. Chen, C. E. Nanayakkara, V. H. Grassian, *Chem. Rev.* **2012**, *112*, 5919–5948.
[7] S. Lacombe, T. Pigot, *Catal. Sci. Technol.* **2016**, *6*, 1571–1592.
[8] M. A. Henderson, *J. Surf. Sci. Rep.* **2011**, *66*, 185–297.
[9] J. F. Banfied, D. R. Veblen, *J. Am. Mineral.* **1992**, *77*, 545–557.
[10] M. Grätzel, *Nature* **2001**, *414*, 338–344.
[11] A. Fujishima, K. Honda, *Nature* **1972**, *37*, 238–242.
[12] P. K. Dutta, A. Ginwalla, B. Hogg, B. R. Patton, B. Chwieroth, Z. Liang, P. Gouma, M. Mills, S. Akbar, *J. Phys. Chem.* **1999**, *103*, 4412–4422.
[13] M. Hayyan, M. A. Hashim, I. N. AlNashef, *Chem. Rev.* **2016**, *116*, 3029–3085.
[14] Y. Nosaka, A. Y. Nosaka, *Chem. Rev.* **2017**, *117*, 11302–11336.
[15] W. Kim, T. Tachikawa, G. Moon, T. Majima, W. Choi, *Angew. Chem. Int. Ed. Engl.* **2014**, *126*, 14260–14265.
[16] M. Buchalska, M. Kobielusz, A. Matuszek, M. Pacia, S. Wojtyla, W. Macyk, *ACS Catal.* **2015**, *5*, 7424–7431.
[17] a) A. Aronne, M. Fantauzzi, C. Imparato, D. Atzei, L. De Stefano, G. D'Errico, F. Sannino, I. Rea, D. Pirozzi, B. Elsener, P. Pernice, A. Rossi, *RSC Adv.* **2017**, *7*, 2373–2381; b) F. Sannino, P. Pernice, C. Imparato, A. Aronne, G. D'Errico, L. Minieri, M. Perfetti, D. Pirozzi, *RSC Adv.* **2015**, *5*, 93831–93839.
[18] H. Tang, H. Berger, P. E. Schmid, F. Lévy, G. Burri, *Solid State Commun.* **1993**, *87*, 847–850.
[19] L. Zang, W. Macyk, C. Lange, W. F. Maiser, C. Antonius, D. Meissner, H. Kisch, *Chem. A Eur. J.* **2000**, *2*, 379–384.
[20] X. Z. Li, F. B. Li, *Environ. Sci. Technol.* **2001**, *35*, 2381–2387.
[21] W. Navarra, I. Ritacco, O. Sacco, L. Caporaso, M. Farnesi Camellone, V. Venditto, V. Vaiano, *J. Phys. Chem. C* **2022**, *126*, 7000–7011.
[22] I. Ritacco, O. Sacco, L. Caporaso, M. Farnesi Camellone, *J. Phys. Chem. C* **2022**, *126*, 3180–3193.
[23] A. P. Singh, N. Kodan, B. R. Mehta, A. Held, L. Mayrhofer, M. Moseler, *ACS Catal.* **2016**, *6*, 5311–5318.
[24] Y. Bessekhouad, D. Robert, J. V. Weber, *Catal. Today* **2005**, *101*, 315–321.
[25] J. Resasco, H. Zhang, N. Kornienko, N. Becknell, H. Lee, J. Guo, A. L. Briseno, P. Yang, *ACS Cent. Sci.* **2016**, *2*, 80–88.
[26] I. Ritacco, C. Imparato, L. Falivene, L. Cavallo, A. Magistrato, L. Caporaso, M. Farnesi Camellone, A. Aronne, *Adv. Mater. Interfaces* **2021**, *8*, 2100629.
[27] Y. Wang, B. Wen, A. Dahal, G. A. Kimmel, R. Rousseau, A. Selloni, N. G. Petrik, Z. Dohnálek, *J. Phys. Chem. C* **2020**, *124*, 20228–20239.
[28] L. M. Liu, S. C. Li, H. Cheng, U. Diebold, A. Selloni, *J. Am. Chem. Soc.* **2011**, *133*, 7816–7823.
[29] M. Setvin, X. Shi, J. Hulva, T. Simschitz, G. S. Parkinson, M. Schmid, C. Di Valentin, A. Selloni, U. Diebold, *ACS Catal.* **2017**, *7*, 7081–7091.
[30] O. V. Makarova, T. Rajh, M. C. Thurnauer, A. Martin, P. A. Kemme, D. Cropek, *Environ. Sci. Technol.* **2000**, *34*, 4797–4803.
[31] T. Rajh, J. M. Nedeljkovic, L. X. Chen, O. Poluektov, M. C. Thurnauer, *J. Phys. Chem. B* **1999**, *103*, 3515–3519.
[32] A. P. Xagas, M. C. Bernard, A. Hugot-Le Goff, N. Spyrellis, Z. Loizos, P. Falaras, *J. Photochem. Photobiol. A* **2000**, *132*, 115–120.
[33] Y. Ou, J. D. Lin, H. M. Zou, D. W. Liao, *J. Mol. Catal. A* **2005**, *241*, 59–64.
[34] A. Abbasi, J. J. Sardroodi, *J. Nanoanalysis* **2018**, *5(1)*, 36–48.
[35] V. Bajić, B. Spremo-Potparević, L. Živković, A. Čabarkapa, J. Kotur-Stevuljević, E. Isenović, D. Sredojević, I. Vukoje, V. Lazić, S. P. Ahrenkiel, J. M. Nedeljković, *Colloids Surf. B* **2017**, *155*, 323–331.
[36] E. H. Mert, Y. Yalçın, M. Kılıç, N. San, Z. Çınar, *J. Adv. Oxid. Technol.* **2008**, *11(2)*, 199–207.
[37] K. L. Miller, C. W. Lee, J. L. Falconer, J. W. Medlin, *J. Catal.* **2010**, *275*, 294–299.
[38] L. F. Liao, W. C. Wu, C. Y. Chen, J. L. Lin, *J. Phys. Chem. B* **2001**, *105*, 7678–7685.
[39] F. P. Rotzinger, J. M. Kesselman-Truttmann, S. J. Hug, V. Shklover, M. Gratzel, *J. Phys. Chem. B* **2004**, *108*, 5004–5017.
[40] M. Xu, H. Noei, M. Buchholz, M. Muhler, C. Wöll, Y. Wang, *Catal. Today* **2012**, *182*, 12–15.
[41] C. E. Nanayakkara, J. K. Dillon, V. H. Grassian, *J. Phys. Chem. C* **2014**, *118*, 25487–25495.
[42] B. Wen, A. Selloni, *J. Phys. Chem. Lett.* **2021**, *12*, 6840–6846.

[43] J. VandeVondele, M. Krack, F. Mohamed, M. Parrinello, T. Chassaing, J. Hutter, *Comput. Phys. Commun.* **2005**, *167*, 103–128.
[44] J. P. Perdew, K. Burke, Y. Wang, *Phys. Rev. B* **1996**, *54*, 16533–16539.
[45] J. VandeVondele, J. Hutter, *J. Chem. Phys.* **2007**, *127*, 114105.
[46] S. Goedecker, M. Teter, J. Hutter, *Phys. Rev. B* **1996**, *54*, 1703–1710.
[47] O. A. Vydrov, T. Van Voorhis, *J. Chem. Phys.* **2010**, *133*, 244103.
[48] R. Sabatini, T. Gorni, S. de Gironcoli, *Phys. Rev. B* **2013**, *87*, 041108.
[49] G. Miceli, S. d Gironcoli, A. Pasquarello, *J. Chem. Phys.* **2015**, *142*, 034501.
[50] G. A. Gamov, D. N. Yarullin, M. A. Gudyrina, E. I. Pogodina, A. S. Medvedeva, M. N. Zavalishin, *J. Chem. Eng. Data* **2022**, *67*, 1358–1364.
[51] F. Fasulo, G. M. Piccini, A. B. Muñoz-García, M. Pavone, M. Parrinello, *J. Phys. Chem. C* **2022**, *126(37)*, 15752–15758.
[52] W. Tang, E. Sanville, G. Henkelman, *J. Phys. Condens. Matter.* **2009**, *21*, 084204.
[53] E. Sanville, S. D. Kenny, R. Smith, G. Henkelman, *J. Comput. Chem.* **2007**, *28*, 899–908.
[54] G. Henkelman, A. Arnaldsson, H. Jònsson, *Comput. Mater. Sci.* **2006**, *36*, 354–360.
[55] A. Calzolari, G. Cicero, C. Cavazzoni, R. Di Felice, A. Catellani, S. Corni, *J. Am. Chem. Soc.* **2010**, *132*, 4790–4795.
[56] P. H.-L. Sit, N. Marzari, *J. Chem. Phys.* **2005**, *122*, 204510.
[57] J. C. Grossman, E. S. Schwegler, E. W. Draeger, F. Gygi, G. Galli, *J. Chem. Phys.* **2004**, *120*, 300–311.
[58] G. Bussi, D. Donadio, M. Parrinello, *J. Chem. Phys.* **2007**, *126*, 014101.
[59] L. Szabová, M. Farnesi Camellone, F. N. Ribeiro, V. Matolìn, Y. Tateyama, S. Fabris, *J. Phys. Chem. C* **2018**, *122*, 27507–27515.
[60] M. Farnesi Camellone, D. Marx, *J. Phys. Chem. Lett.* **2013**, *4*, 514–518.
[61] P. Schienbien, D. Marx, *J. Phys. Chem. B* **2018**, *122*, 3318–3329.
[62] J. P. W. Treacy, H. Hussain, X. Torrelles, D. C. Grinter, G. Cabailh, O. Bikondoa, C. Nicklin, S. Selcuk, A. Selloni, R. Lindsay, G. Thornton, *Phys. Rev. B* **2017**, *95*, 075416.
[63] R. Zhang, Z. Liu, L. Ling, B. Wang, *Appl. Surf. Sci.* **2015**, *353*, 150–157.
[64] M. Farnesi Camellone, F. N. Ribeiro, L. Szabová, Y. Tateyama, S. Fabris, *J. Am. Chem. Soc.* **2016**, *138*, 11560–11567.
[65] I. M. Nadeem, J. P. W. Treacy, S. Selcuk, X. Torrelles, H. Hussain, A. Wilson, D. C. Grinter, G. Cabailh, O. Bikondoa, C. Nicklin, A. Selloni, J. Zegenhagen, R. Lindsay, G. Thornton, *J. Phys. Chem. Lett.* **2018**, *9*, 3131–3136.
[66] Z. Geng, X. Chen, W. Yang, Q. Guo, C. Xu, D. Dai, X. Yang, *J. Phys. Chem. C* **2016**, *120*, 26807–26813.
[67] M. Fronzi, S. Piccinin, B. Delley, e. Traversa, C. Stampfl, *Phys. Chem. Chem Phys.* **2009**, *11*, 9188–9199.
[68] R. Xu, Z. Zhou, Y. Wang, H. Xiao, L. Xu, Y. Ding, X. Li, A. Li, G. Fang, *Nanomaterials* **2022**, *12*, 4362.
[69] B. Meyer, D. Marx, O. Dulub, U. Diebold, M. Kunat, D. Langenberg, C. Wöll, *Angew. Chem. Int. Ed.* **2004**, *43*, 6642–6645.
[70] M. F. Calegari Andrade, H. Y. Ko, L. Zhang, R. Car, A. Selloni, *Chem. Sci.* **2020**, *11*, 2333–2341.
[71] J. Liu, Y. Liu, J. Yang, X. C. Zeng, X. He, *J. Phys. Chem. Lett.* **2021**, *12*, 3379–3386.

Manuscript received: October 17, 2023
Revised manuscript received: December 16, 2023
Accepted manuscript online: December 28, 2023
Version of record online: January 10, 2024